RSC Advances

PAPER

View Article Online
View Journal | View Issue

Cite this: *RSC Adv.*, 2025, **15**, 9884

Direct detection of lymphoma cancer cells based on impedimetric immunosensors

Asghar Barani Beiranvand,[a] Fariba Tadayon *[a] and Hasan Bagheri[b]

This study focuses on the creation and application of an advanced impedimetric immunosensor designed for the sensitive detection of lymphoma cancer cells. The sensor was developed by modifying a glassy carbon electrode (GCE) with gold nanoparticles (AuNPs) and 3,3′-dithiodipropionic acid di(*N*-hydroxysuccinimide ester) boronic acid (AuNPs@DTSP–BA), followed by the attachment of rituximab monoclonal antibody. Incorporating the boronic acid (BA) component enabled effective oriented immobilization of the antibody, thereby improving the performance of the biosensor. Various spectroscopic techniques were used to characterize the immunosensor. The developed immunosensor demonstrated the ability to detect lymphoma cancer cells across a wide linear range of 100 to 50 000 cells per mL, with a detection sensitivity of 64 cells per mL.

Received 1st November 2024
Accepted 10th February 2025

DOI: 10.1039/d4ra07801b

rsc.li/rsc-advances

1. Introduction

Cancer is marked by the unregulated growth of malignant cells in different tissues and continues to be one of the foremost causes of death globally, with incidence rates steadily increasing.[1] Early detection is crucial for effective treatment and significantly improves survival rates, as it can identify cancer at its nascent stages and enhance treatment outcomes. Early cancer biomarkers encompass detectable structural changes in tissues as well as biochemical modifications. Despite advancements, developing technologies sensitive enough to detect early tumors while minimizing false positives remains challenging. Recent advancements are enhancing early cancer detection by targeting tumor metabolites and by-products, often more prevalent than the tumor cells themselves. Increased sensitivity is achieved through specialized probes, such as tumor-specific antibodies or peptides labeled with radioisotopes, which amplify detection signals.[2]

Advancements in miniaturized sensor technology and novel sensing substrates propel electrochemical biosensors towards portable and point-of-care (POC) applications, thus reducing dependence on complex laboratory setups. Biosensors are analytical devices designed to translate biorecognition events into measurable physicochemical signals. There is growing interest in developing cost-effective and innovative strategies with higher sensitivity and selectivity for clinically relevant biomarkers. Electrochemical immunosensing strategies are particularly promising due to their combination of antibody specificity and rapid response times, making them valuable for real-time clinical testing.[3]

For creating robust and sensitive immunosensors, covalent, site-specific immobilization of antibodies is crucial. Boronic acid (BA) forms reversible cyclic boronate bonds with 1,2-diols and 1,3-diols, providing strong adsorption affinity and specificity for carbohydrate chains, particularly in the Fc region. This property aids in accurately extracting biomarkers from human serum, minimizing interference.[4] Enhancing electron exchange in electrochemical sensors involves integrating highly electrocatalytic and conductive materials. Recent advances in nanotechnology have brought significant attention to the use of nanomaterials, such as metal nanoparticles, carbon nanomaterials, and quantum dots, to modify electrochemical sensors for improved performance.[5–7]

CD20 is an antigen specific to B cells. It is found on mature B cells and the majority of non-Hodgkin's lymphomas, while it is not present on early progenitors or mature plasma cells. CD20 serves as a critical target for antibody-based therapies in treating non-Hodgkin's lymphoma (NHL) and B-cell chronic lymphocytic leukemia (B-CLL). Rituximab, a chimeric monoclonal antibody incorporating murine and human components, specifically targets the CD20 antigen.[8] Electrochemical immunosensors have recently gained considerable interest in disease diagnosis and monitoring. Detection of analytes with electrochemical techniques, a popular approach is driving the enhancement of sensitivity with signal amplification. Electrochemical affinity biosensors have been attractive for a broad range of applications in clinical diagnosis, biomedical research, food quality control and environmental monitoring because of their simplicity, rapid response, and compatibility with miniaturization. In particular, electrochemical immunosensors, relying on the specific antigen–antibody interaction, are the most widely used thanks to some of their peculiar features. Here, we take advantage of the rituximab monoclonal anti-CD20 antibody which specifically binds to the B cells membrane

[a]*Department of Chemistry, Islamic Azad University, North Tehran Branch, Tehran, Iran. E-mail: f_tadayon@iau-tnb.ac.ir*

[b]*Chemical Injuries Research Center, Systems Biology and Poisonings Institute, Baqiyatallah University of Medical Sciences, Tehran, Iran*

surface, to introduce a novel strategy for specific detection of lymphomas cancer cells. Electrochemical impedance spectroscopy (EIS) offers a label-free, sensitive approach to studying surface phenomena and bulk property changes, providing a non-destructive method to characterize biological interfaces.

While flow cytometry offers higher accuracy and multiparameter analysis, impedance sensing provides a cost-effective, rapid, and non-invasive alternative for detecting lymphoma cancer cells. Impedance sensing is generally more affordable, making it accessible for routine use and large-scale studies. Additionally, it is label-free, which reduces the complexity and cost of sample preparation. The method enables real-time monitoring, providing faster analysis and immediate results.[9,10]

EIS enables the direct detection of immunospecies by analyzing interactions between immobilized biological components and analytes.[11] Carbon-based electrodes, such as glassy carbon electrodes (GCE), carbon paste electrodes, and screen-printed electrodes, are widely utilized in electrochemical systems. Their popularity is due to their affordability, stability, and ease of modification.[12]

In this study, an impedimetric immunosensor was developed to detect lymphoma cancer cells. The sensor was constructed by modifying the GCE surface with AuNPs@DTSP–BA nanocomposites and subsequently immobilizing rituximab monoclonal antibody on the modified surface. The resulting immunosensor demonstrated high sensitivity and the ability to detect and quantify cancer cells effectively.

2. Experimental

2.1. Materials and equipment

High-purity reagents from Merck were used throughout the study without additional purification. Phosphate buffer solution (PBS, 0.1 M) was prepared by dissolving NaCl, KCl, KH_2PO_4, and $Na_2HPO_4 \cdot 2H_2O$, with pH adjustments made using diluted NaOH or HCl. All solutions were prepared using double-distilled water (DDW). The chemicals 3,3′-dithiodipropionic acid di(*N*-hydroxysuccinimide ester) (DTSP), dimethylformamide (DMF), $HAuCl_4 \cdot 3H_2O$, citric acid, bovine serum albumin (BSA), boronic acid (BA), $K_3[Fe(CN)_6]$, and $K_4[Fe(CN)_6]$ were obtained from Merck.

Electrochemical measurements were performed using an Ivium Vertex potentiostat/galvanostat (Ivium Technologies, The Netherlands). The electrochemical cell setup included a modified GCE as the working electrode, an Ag/AgCl reference electrode, and a platinum wire counter electrode. For EIS, a sine wave potential with an amplitude of 10 mV was applied over a frequency range from 0.1 Hz to 100 kHz. Fourier-transform infrared (FT-IR) spectra of the synthesized nanocomposite were recorded with a Shimadzu-8400S spectrometer. The nanocomposite morphology was examined using transmission electron microscopy (TEM).

2.2. Preparation of the AuNPs, AuNPs@DTSP and AuNPs@DTSP–BA nanocomposites

Gold nanoparticles were synthesized using the well-known citrate reduction method of gold salt. In this process, a solution of $HAuCl_4 \cdot 3H_2O$ (100 mL, 10 mM) was stirred at a rate of approximately 700 rpm while being heated to boiling. Once boiling, a trisodium citrate solution (10 mL, 38.8 mM) was rapidly added. The mixture was then boiled for an additional 20 minutes before the heating was stopped, allowing the solution to cool to room temperature. The resulting gold nanoparticles were stored at 4 °C until further use.

To functionalize the synthesized nanoparticles, 200 μL of a 2 mM DTSP solution in DMF was added to 100 mL of the gold nanoparticle solution and stirred for 45 minutes.[13] This step facilitated the attachment of boronic acid to the surface of the AuNPs@DTS nanocomposite through a reaction between the amino group of the boronic acid and the ester group of the nanocomposite, forming an amide bond. Following this, the AuNPs@DTS were isolated by centrifugation, resuspended in PBS, and then treated with a 0.1% boronic acid (BA) solution for 2 hours.[14–17] The resulting AuNPs@DTS–BA were centrifuged, washed with water, and dispersed in PBS. The final product was stored at 4 °C until needed for sensing applications.[8]

2.3. Preparation of proposed immunosensor

The GCE was initially cleaned through mechanical polishing with an alumina slurry, followed by sonication in water and ethanol. The cleaned electrode was then dried at ambient temperature. A 10 μL drop of the synthesized AuNPs@DTS–BA nanocomposite was applied to the dried GCE surface and allowed to dry at room temperature. Once dried, the electrode was rinsed with phosphate buffer. Subsequently, a 10 μL drop of an antibody solution, prepared at a concentration of 100 μg mL^{-1}, was added to the modified electrode surface and incubated for 4 hours at 4 °C, with the electrode covered to prevent evaporation.

After incubation, the electrode was rinsed with phosphate buffer to remove any unbound antibodies. A 0.05% (w/v) bovine serum albumin (BSA) solution was applied and incubated for 1 hour to minimize non-specific binding and block remaining active sites on the electrode surface. The final biosensor was then exposed to various concentrations of cancer cells, and the resulting signals were recorded.

2.4. Preparation of real samples

For real sample analysis, the residual whole blood samples from two cancer patients were obtained from a clinical laboratory, after anonymization. They were used without any further treatment to evaluate the biosensor's performance in real-world applications.

3. Results and discussion

3.1. Morphological and spectral properties of AuNPs, AuNPs@DTSP, and AuNPs@DTSP–BA nanocomposites

AuNPs are favored in analytical methods due to their unique optical characteristics, ease of synthesis, and compatibility with biological systems. These properties make AuNPs ideal for the precise detection of various analytes.

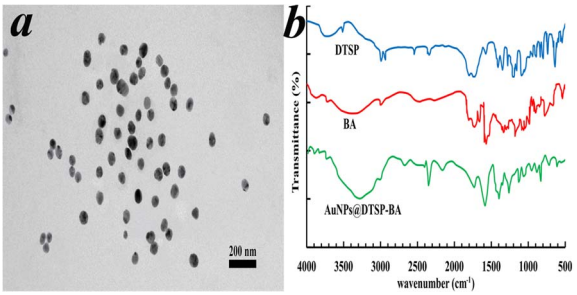

Fig. 1 Characterization of the synthesized nanocomposite. (a) TEM image of AuNPs@DTSP–BA, (b) FT-IR spectra of DTSP, BA and AuNPs@DTSP–BA

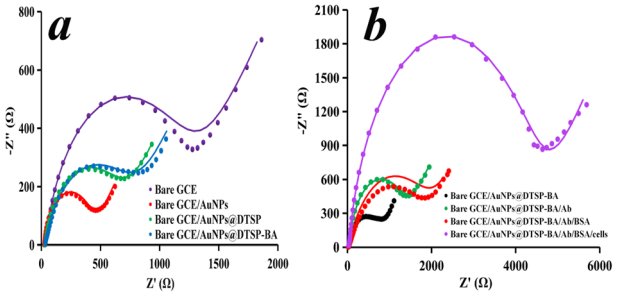

Fig. 2 Nyquist plots at different modification steps of (a) the nanocomposite surface and (b) the immunosensor fabrication. Dot and line plots related to experimental and fitted data, respectively. EISs measurements were carried out in PBS containing KCl (0.1 M) and $[Fe(CN)_6]^{3-/4-}$ (5 mM).

In this study, the AuNPs@DTSP–BA nanocomposite was characterized using the TEM, with representative images provided in Fig. 1a. The TEM analysis revealed that the average diameter of the nanoparticles was approximately 55.9 nm. Additionally, FTIR was employed to analyze the surface chemistry of the nanocomposite, with the spectra displayed in Fig. 1b. The FTIR spectra showed peaks at 2556 and 740 cm^{-1}, which correspond to the S–H and S–C bonds in DTSP. However, the thiol peak at 2556 cm^{-1} was missing in the AuNPs@DTSP–BA spectrum, suggesting that the DTSP ligand was effectively functionalized on the AuNPs. Peaks at 1585 and 1260 cm^{-1}, associated with the C=O and N–O groups of DTSP, remained present, indicating partial retention of these functional groups. Furthermore, the spectrum exhibited bands between 1360 and 1060 cm^{-1} and 1032 and 730 cm^{-1} corresponding to the bending vibrations of the C–H bonds. The peak at 3000 cm^{-1} was attributed to the C–H stretching in the aromatic ring, confirming the successful incorporation of boronic acid onto the nanocomposite surface.

3.2. Electrochemical analysis of AuNPs@DTSP–BA nanocomposites using EIS

EIS is a critical technique for evaluating the electrochemical characteristics of modified electrode surfaces. EIS provides high sensitivity to alterations at the electrode–electrolyte interface by applying an alternating signal over a range of frequencies, with results commonly depicted in Nyquist, Bode, or Cole–Cole plots. These plots are analyzed using theoretical equivalent circuit models to understand the electrochemical reactions at the interface. The Randles equivalent circuit is often employed for such analyses, incorporating elements like electrolyte resistance (R_s), double-layer capacitance (C_{dl}) or constant phase element (CPE), charge transfer resistance (RCT), and Warburg impedance (W).

This study utilized EIS to monitor changes in the AuNPs@DTSP–BA nanocomposite. The impedance data for the modified electrodes were fitted to the Randles equivalent circuit model. The charge transfer resistance (RCT) is a crucial indicator of the insulating properties at the electrode/electrolyte interface and is essential for evaluating the immunosensor's performance.

To validate the fabrication process of the AuNPs@DTSP–BA nanocomposite, we measured changes in resistance on the GCE surface at each modification stage. Initially, AuNPs were deposited on the GCE, followed by measurements of RCT. Subsequent deposits of AuNPs@DTSP and AuNPs@DTSP–BA were made, with Nyquist plots generated for each step. These plots were analyzed using a modified Randles equivalent circuit, as shown in Fig. 2a. The experimental and fitted impedance spectra demonstrated strong consistency, with less than 5% fitting errors, as detailed in Table 1. The RCT increased sequentially from 405 Ω to 638 Ω and 737 Ω after each modification, indicating successful and robust functionalization of the AuNPs.

Table 1 Obtained Randles parameters for the fabrication steps of the proposed nanocomposite

	R_{CT} (Ω)	R_s (Ω)	Q (μMho)	N	W (μMho)
Bare GCE	1190	34.6	10.3	0.851	774
GCE/AuNPs	405	23.8	9.44	0.895	1680
GCE/AuNPs@DTSP	638	30.8	17.6	0.824	1070
GCE/AuNPs@DTSP–BA	737	33.8	20.0	0.757	618

Gold nanoparticles are widely recognized in electroanalytical applications due to their high surface-to-volume ratio, rapid electron transfer capabilities, and biocompatibility. DTSP facilitates effective self-assembly and covalent bonding with biomolecules on gold surfaces with its disulfide and succinimidyl groups. Boronic acid (BA) derivatives are useful linkers in immunosensor technology, and their successful attachment is critical for sensor functionality. BA was covalently linked to the AuNPs@DTSP surface *via* amide bond formation between BA's amine and DTSP's succinimidyl groups in this study.

The RCT for the GCE/AuNPs was lower than the bare GCE, attributed to the enhanced surface area and electrical conductivity of the AuNPs. The increase in RCT upon formation of AuNPs@DTSP and further with AuNPs@DTSP–BA confirmed the effective immobilization of DTSP and BA, reflecting the insulating nature of these components.

3.3. Electrochemical characterization of proposed immunosensor

The EIS technique was used to validate the successful modification of the electrode throughout the immunosensor

Table 2 Obtained Randles parameters for the fabrication steps of the proposed immunosensor, related to Fig. 2b

	R_{CT} (Ω)	R_s (Ω)	Q (μMho)	N	W (μMho)
GCE/AuNPs@DTSP–BA/Ab	1310	36	7.20	0.893	585
GCE/AuNPs@DTSP–BA/Ab/BSA	1970	22.6	26.7	0.687	1100
GCE/AuNPs@DTSP–BA/Ab/BSA/cells[a]	4440	32	2.68	0.871	485

[a] C_{cells} = 3000 cells per mL.

fabrication process. In Nyquist plots, the diameter of the semicircle represents the charge transfer resistance (RCT). This resistance is inversely related to the electron transfer rate, meaning that a larger semicircle diameter indicates a lower electron transfer rate and *vice versa*. Additionally, the lower frequency region of the plot highlights limitations imposed by the diffusion process.[18]

As shown in Fig. 2b, a decrease in RCT was observed after applying the AuNPs@DTSP–BA nanocomposite to the GCE surface.[19–23] This reduction is attributed to the large surface area provided by the nanostructure, which enhances electron transfer. Boronic acids (BAs) are particularly effective in the oriented immobilization of antibodies. BA demonstrates excellent potential for antibody immobilization, offering advantages such as self-assembly with antibodies and orientation-controlled arrangement, which exposes the antigen-binding site.[24] Immobilizing rituximab antibodies on the modified electrode surface led to a significant increase in RCT.[25–27]

This increase indicates successful antibody immobilization, as the redox probe's accessibility was reduced, and electron transfer was hindered.[28]

An ideal blocking reagent must occupy all remaining non-specific binding (NSB) sites after the coated protein is adsorbable. Bovine serum albumin (BSA) is the most commonly used blocking reagent.[29]

As shown in Fig. 2b, the RCT value increased further after blocking non-specific binding (NSB) sites with BSA. When the immunosensor was incubated with cancer cells, the RCT increased additionally due to the formation of an insulating layer on the electrode surface. The impedance data were fitted using the equivalent circuit model, with the resulting values presented in Table 2. These values were achieved with a relative error of less than 5%.

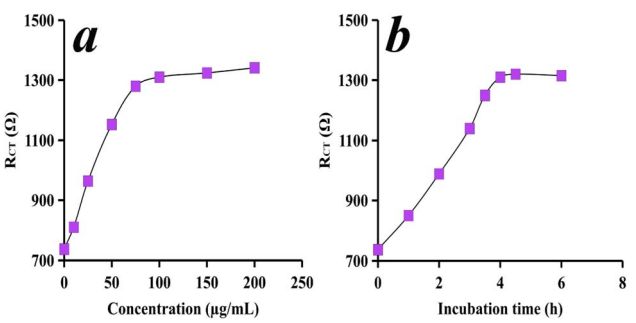

Fig. 3 Optimization of incubation (a) concentration and (b) time of immobilization of Ab.

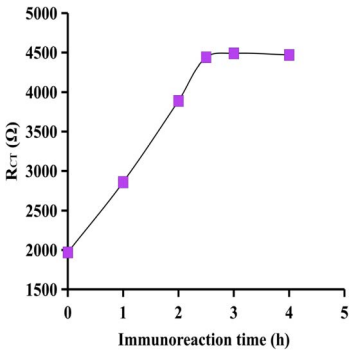

Fig. 4 Optimization of the immunoreaction time (C_{cells} = 3000 cells per mL).

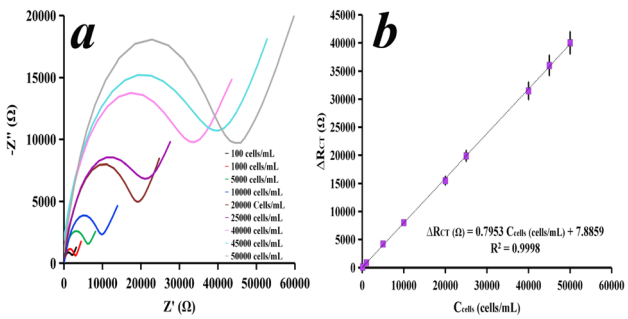

Fig. 5 (a) Nyquist plots of immunosensor incubated with different lymphoma cancer cells, and (b) calibration curve of impedimetric immunosensor for cancer cell detection.

3.4. Optimization of conditions for antibody immobilization

EIS was utilized with accuracy to determine the ideal antibody concentration and incubation time for optimal immunosensor

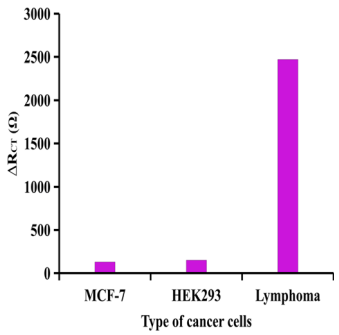

Fig. 6 EIS results for control experiments of immunosensor.

Table 3 Detection of lymphoma cancer cell in real samples by proposed and reported method

Sample	Found (cells per mL)	RSD	Flow cytometry method[8,31] (cells per mL)
Blood sample 1	350	4	380[a]
Blood sample 2	570	3.6	510[a]

[a] The samples and results are the same as the ones reported in ref. 8 and 31.

performance. As illustrated in Fig. 3a, the RCT value increased steadily with antibody concentration, reaching a 100 μg mL^{-1} peak. Beyond this concentration, no significant increase in charge transfer resistance was observed. Hence, 100 μg mL^{-1} was the optimal antibody concentration for sensor fabrication. Similarly, Fig. 3b demonstrates that the RCT value increased with incubation time, reaching a peak at 4 hours before leveling off, a precise finding. Therefore, 4 hours was selected as the ideal incubation period, a precise conclusion drawn from the research.

3.5. Optimization of immunoreaction time

Immunoreaction time is a crucial factor affecting the sensitivity of an immunoassay.[30] To determine the optimal duration, we investigated the impact of immunoreaction times ranging from 1 to 4 hours on the interaction between rituximab and cancer cells. The results in Fig. 4 indicate that the RCT value increased with more extended incubation periods, peaking at 2.5 hours before leveling off. Thus, 2.5 hours was the optimal immunoreaction time for interacting antibodies and cancer cells.

3.6. Performance evaluation of the immunosensor

The performance of the immunosensor was assessed under optimal conditions by measuring its response to different concentrations of cancer cells. As illustrated in Fig. 5a, the EIS responses of the immunosensors showed a progressive increase in the charge transfer resistance (RCT) with higher cancer cell concentrations. The change in RCT was quantified using the following equation:

$$\Delta\text{RCT} = \text{RCT (GCE/AuNPs@DTSP–BA/Ab/BSA/cells)} - \text{RCT (GCE/AuNPs@DTSP–BA/Ab/BSA)}$$

where RCT (GCE/AuNPs@DTSP–BA/Ab/BSA/cells) is the resistance value of the immunosensor following incubation with cancer cells, and RCT (GCE/AuNPs@DTSP–BA/Ab/BSA) is the resistance value of the immunosensor after blocking with BSA. Fig. 5b demonstrates the relationship between the ΔRCT and the concentration of cancer cells that fit well into a linear regression with the equation $\Delta\text{RCT}\ (\Omega) = 0.7953\ C_{\text{cells}}$ (cells per mL) + 7.8859 ($R2 = 0.9998$) in the range of 100–50 000 cells per mL. The LOD for the immunosensor was determined to be 62 cells per mL.

To assess the immunosensor's reproducibility, three devices were fabricated under identical conditions and tested with a concentration of 3000 cells per mL. The relative standard deviation (RSD) was 3.5%, indicating reliable and consistent performance detecting lymphoma cancer cells.

The immunosensor's storage stability was evaluated by keeping three devices in phosphate-buffered saline (PBS) at 4 °C for seven days. After this storage period, the EIS response showed only a 4.6% decrease compared to the initial measurement, demonstrating that the immunosensor retains its stability over time.

3.7. Control experiments

To evaluate the specificity of the proposed immunosensor for lymphoma cancer cells and its selective binding ability, the immunosensor was tested against two different control human cell lines: breast cancer cells (MCF-7) and human embryonic kidney cells (HEK293), alongside the lymphoma cells.[8,31]

When immunosensor was incubated with the control cells at a concentration of 3000 cells per mL, the RCT values exhibited minimal change. In contrast, incubation with the same concentration of lymphoma cells resulted in a significant increase in RCT. These findings demonstrate the immunosensor's high selectivity for detecting lymphoma cancer cells over other cell types. The variations in ΔRCT in response to different cell types are shown in Fig. 6.

3.8. Analysis of real samples

In this study, human blood samples were used as a model of complex systems, and cancer cells were analyzed as one type of CTCs within these samples.[8,31] In order to examine the applicability of the proposed immunosensor in analyzing real samples, we used two blood samples that had previously been analyzed by standard methods and their results had been reported in the papers of Bagheri *et al.*[8,31] The results demonstrated good agreement between the two methods, with no significant differences (at a 95% confidence limits), indicating that the suggested strategy can be appropriated for lymphoma cancer cells determination in blood samples. Notably, this approach is effective without significant matrix interference from the real sample, making the immunosensor especially suitable for the early diagnosis of lymphoma cancer. The obtained results were shown in Table 3.

4. Conclusion

In this study, we engineered the AuNPs@DTSP–BA nanocomposite to serve as a surface electrode modifier, aiming to improve signal amplification and support the precise orientation and immobilization of antibodies specific to cancer cells.

The resulting label-free electrochemical immunosensor was utilized to detect and quantify lymphoma cancer cells through EIS. The immunosensor displayed a robust linear relationship between impedance changes and cancer cell concentrations ranging from 100 to 50 000 cells per mL, with a low detection limit of 64 cells per mL. Furthermore, it successfully identified cancer cells in blood samples, underscoring its practical utility and dependability.

Ethical statement

All experiments were performed in accordance with the Guidelines of Iran National Committee for Ethics in Biomedical Research. The research ethics committee of Islamic Azad University, North Tehran Branch, has approved this project (Approval ID: IR.IAU.TNB.REC.1403.273). The residual whole blood samples from two cancer patients were obtained from a clinical laboratory, after anonymization. They were used without any further treatment.

Data availability

All data supporting the findings of this study are included within the article. No additional datasets, software, or code were generated or used during this study.

Conflicts of interest

There are no conflicts to declare.

Acknowledgements

The authors gratefully acknowledge the supports from Research Councils of Islamic Azad University, North Tehran Branch.

References

1 B. Muthazhagan, T. Ravi and D. Rajinigirinath, An enhanced computer-assisted lung cancer detection method using content based image retrieval and data mining techniques, *Journal of Ambient Intelligence and Humanized Computing*, 2020, 1–9.

2 D. Crosby, S. Bhatia, K. M. Brindle, L. M. Coussens, C. Dive, M. Emberton, S. Esener, R. C. Fitzgerald, S. S. Gambhir and P. Kuhn, Early detection of cancer, *Science*, 2022, **375**(6586), eaay9040.

3 G. Manasa, R. J. Mascarenhas, S. J. Malode and N. P. Shetti, Graphene-based electrochemical immunosensors for early detection of oncomarker carcinoembryonic antigen, *Biosens. Bioelectron.: X*, 2022, **11**, 100189.

4 S. Gao, J. M. Guisán and J. Rocha-Martin, Oriented immobilization of antibodies onto sensing platforms-a critical review, *Anal. Chim. Acta*, 2022, **1189**, 338907.

5 F. Tadayon, S. Vahed and H. Bagheri, Au-Pd/reduced graphene oxide composite as a new sensing layer for electrochemical determination of ascorbic acid, acetaminophen and tyrosine, *Mater. Sci. Eng., C*, 2016, (68), 805–813.

6 F. Tadayon and Z. Sepehri, New electrochemical sensor based on nitrogen-doped graphene/$CuCo_2O_4$ nanocomposite for simultaneous determination of dopamine, melatonin and tryptophan, *RSC Adv.*, 2015, **5**(80), 65560.

7 M. Ghanavati, F. Tadayon and H. Bagheri, A novel label-free impedimetric immunosensor for sensitive detection of prostate specific antigen using Au nanoparticles/MWCNTs-graphene quantum dots nanocomposite, *Microchem. J.*, 2020, **159**, 105301.

8 P. Hashemi, A. Afkhami, B. Baradaran, R. Halabian, T. Madrakian, F. Arduini, T. A. Nguyen and H. Bagheri, Well-orientation strategy for direct immobilization of antibodies: development of the immunosensor using the boronic acid-modified magnetic graphene nanoribbons for ultrasensitive detection of lymphoma cancer cells, *Anal. Chem.*, 2020, **92**(16), 11405–11412.

9 Z. Zhang, X. Huang, K. Liu, T. Lan, Z. Wang and Z. Zhu, Recent Advances in Electrical Impedance Sensing Technology for Single-Cell Analysis, *Biosensors*, 2021, **11**(11), 470.

10 Z. Kaleem, Flow Cytometric Analysis of Lymphomas: Current Status and Usefulness, *Arch. Pathol. Lab. Med.*, 2006, **130**(12), 1850–1858.

11 T. A. R. Cordeiro, H. R. Martins, D. L. Franco, F. L. N. Santos, P. A. F. Celedon, V. L. Cantuária, M. de Lana, A. B. Reis and L. F. Ferreira, Impedimetric immunosensor for rapid and simultaneous detection of Chagas and visceral leishmaniasis for point of care diagnosis, *Biosens. Bioelectron.*, 2020, **169**, 112573.

12 M. Ghanavati, F. Tadayon, A. Basiryanmahabadi, N. Torabi Fard and E. Smiley, Design of new sensing layer based on ZnO/NiO/Fe_3O_4/MWCNTs nanocomposite for simultaneous electrochemical determination of Naproxen and Sumatriptan, *J. Pharm. Biomed. Anal.*, 2023, **223**, 115091.

13 T. J. Jayeoye, T. Kangkamano and T. Rujiralai, Exploiting the high conjugation capacity of creatinine on 3,3′-dithiodipropionic acid di(N-hydroxysuccinimide ester) functionalized gold nanoparticles towards sensitive determination of mercury(II) ion in water, *J. Nanostruct. Chem.*, 2022, **12**(2), 263–276.

14 A. P. Lima, W. T. dos Santos, E. Nossol, E. M. Richter and R. A. Munoz, Critical evaluation of voltammetric techniques for antioxidant capacity and activity: presence of alumina on glassy-carbon electrodes alters the results, *Electrochim. Acta*, 2020, **358**, 136925.

15 W. Sheng, T. Chen, R. Kamath, X. Xiong, W. Tan and Z. H. Fan, Aptamer-enabled efficient isolation of cancer cells from whole blood using a microfluidic device, *Anal. Chem.*, 2012, **84**(9), 4199–4206.

16 T. J. Jayeoye and T. Rujiralai, Sensitive and selective colorimetric probe for fluoride detection based on the interaction between 3-aminophenylboronic acid and dithiobis(succinimidylpropionate) modified gold nanoparticles, *New J. Chem.*, 2020, **44**(15), 5711–5719.

17 S. Mohapatra, N. Panda and P. Pramanik, Boronic acid functionalized superparamagnetic iron oxide nanoparticle as a novel tool for adsorption of sugar, *Mater. Sci. Eng., C*, 2009, **29**(7), 2254–2260.
18 M. Jozghorbani, M. Fathi, S. H. Kazemi and N. Alinejadian, Determination of carcinoembryonic antigen as a tumor marker using a novel graphene-based label-free electrochemical immunosensor, *Anal. Biochem.*, 2021, **613**, 114017.
19 R. Saxena and S. Srivastava, An insight into impedimetric immunosensor and its electrical equivalent circuit, *Sens. Actuators, B*, 2019, **297**, 126780.
20 A.-E. Radi, X. Munoz-Berbel, V. Lates and J.-L. Marty, Label-free impedimetric immunosensor for sensitive detection of ochratoxin A, *Biosens. Bioelectron.*, 2009, **24**(7), 1888–1892.
21 C. Akkapinyo, P. Khownarumit, D. Waraho-Zhmayev and R. P. Poo-Arporn, Development of a multiplex immunochromatographic strip test and ultrasensitive electrochemical immunosensor for hepatitis B virus screening, *Anal. Chim. Acta*, 2020, **1095**, 162–171.
22 A. V. Police Patil, Y.-S. Chuang, C. Li and C.-C. Wu, Recent advances in electrochemical immunosensors with nanomaterial assistance for signal amplification, *Biosensors*, 2023, **13**(1), 125.
23 S. K. Arya, A. Singh, R. Naidoo, P. Wu, M. T. McDermott and S. Evoy, Chemically immobilized T4-bacteriophage for specific Escherichia coli detection using surface plasmon resonance, *Analyst*, 2011, **136**(3), 486–492.
24 P.-H. Lin, S.-C. Huang, K.-P. Chen, B.-R. Li and Y.-K. Li, Effective construction of a high-capacity boronic acid layer on a quartz crystal microbalance chip for high-density antibody immobilization, *Sensors*, 2018, **19**(1), 28.
25 A. Afkhami, P. Hashemi, H. Bagheri, J. Salimian, A. Ahmadi and T. Madrakian, Impedimetric immunosensor for the label-free and direct detection of botulinum neurotoxin serotype A using Au nanoparticles/graphene-chitosan composite, *Biosens. Bioelectron.*, 2017, **93**, 124–131.
26 S. K. Arya, G. Chornokur, M. Venugopal and S. Bhansali, Antibody functionalized interdigitated μ-electrode (IDμE) based impedimetric cortisol biosensor, *Analyst*, 2010, **135**(8), 1941–1946.
27 A. Vasudev, A. Kaushik and S. Bhansali, Electrochemical immunosensor for label free epidermal growth factor receptor (EGFR) detection, *Biosens. Bioelectron.*, 2013, **39**(1), 300–305.
28 A. Attar, J. Mandli, M. M. Ennaji and A. Amine, Label-free electrochemical impedance detection of rotavirus based on immobilized antibodies on gold sononanoparticles, *Electroanalysis*, 2016, **28**(8), 1839–1846.
29 J. E. Contreras-Naranjo and O. Aguilar, Suppressing non-specific binding of proteins onto electrode surfaces in the development of electrochemical immunosensors, *Biosensors*, 2019, **9**(1), 15.
30 T.-B. Xin, X. Wang, H. Jin, S.-X. Liang, J.-M. Lin and Z.-J. Li, Development of magnetic particle-based chemiluminescence enzyme immunoassay for the detection of 17β-estradiol in environmental water, *Appl. Biochem. Biotechnol.*, 2009, **158**, 582–594.
31 F. Fazlali, P. Hashemi, S. M. Khoshfetrat, R. Halabian, B. Baradaran, M. Johari-Ahar, P. Karami, A. Hajian and H. Bagheri, Electrochemiluminescent biosensor for ultrasensitive detection of lymphoma at the early stage using CD20 markers as B cell-specific antigens, *Bioelectrochemistry*, 2021, **138**, 107730.